

1 **Ensemble models from machine learning: an example of wave runup**
2 **and coastal dune erosion**

3 Tomas Beuzen¹, Evan B. Goldstein², Kristen D. Splinter¹

4 ¹Water Research Laboratory, School of Civil and Environmental Engineering, UNSW Sydney, NSW,
5 Australia

6 ²Department of Geography, Environment, and Sustainability, University of North Carolina at
7 Greensboro, Greensboro, NC, USA

Correspondence to: Tomas Beuzen (t.beuzen@unsw.edu.au)

Keywords: Gaussian Process; Narrabeen-Collaroy; Lidar; swash; dune impact model

8 **Abstract**

9 After decades of study and significant data collection of time-varying swash on sandy beaches, there is
10 no single deterministic prediction scheme for wave runup that eliminates prediction error — even
11 bespoke, locally tuned predictors present scatter when compared to observations. Scatter in runup
12 prediction is meaningful and can be used to create probabilistic predictions of runup for a given wave
13 climate and beach slope. This contribution demonstrates this using a data-driven Gaussian process
14 predictor; a probabilistic machine learning technique. The runup predictor is developed using one year of
15 hourly wave runup data (8328 observations) collected by a fixed LIDAR at Narrabeen Beach, Sydney,
16 Australia. The Gaussian process predictor accurately predicts hourly wave runup elevation when tested
17 on unseen data with a root mean-squared-error of 0.18 m and bias of 0.02 m. The uncertainty estimates
18 output from the probabilistic GP predictor are then used practically in a deterministic numerical model of
19 coastal dune erosion, which relies on a parameterization of wave runup, to generate ensemble predictions.
20 When applied to a dataset of dune erosion caused by a storm event that impacted Narrabeen Beach in
21 2011, the ensemble approach reproduced ~85% of the observed variability in dune erosion along the 3.5
22 km beach and provided clear uncertainty estimates around these predictions. This work demonstrates how
23 data-driven methods can be used with traditional deterministic models to develop ensemble predictions
24 that provide more information and greater forecasting skill when compared to a single model using a
25 deterministic parameterization; an idea that could be applied more generally to other numerical models
26 of geomorphic systems.

27 1 Introduction

28 Wave runup is important for characterizing the vulnerability of beach and dune systems and coastal
29 infrastructure to wave action. Wave runup is typically defined as the time-varying vertical elevation of
30 wave action above ocean water levels and is a combination of wave swash and wave setup (Holman,
31 1986; Stockdon et al., 2006). Most parameterizations of wave runup use deterministic equations that
32 output a single value for either the maximum runup elevation in a given time period, R_{max} , or the elevation
33 exceeded by 2% of runup events in a given time period, R_2 , based on a given set of input conditions. In
34 the majority of runup formulae, these input conditions are easily obtainable parameters such as significant
35 wave height, peak wave period, and beach slope (Atkinson et al., 2017; Holman, 1986; Hunt, 1959;
36 Ruggiero et al., 2001; Stockdon et al., 2006). However, wave dispersion (Guza and Feddersen, 2012),
37 wave spectrum (Van Oorschot and d'Angremond, 1969), nearshore morphology (Cohn and Ruggiero,
38 2016), bore-bore interaction (García-Medina et al., 2017), tidal stage (Guedes et al., 2013), and a range
39 of other possible processes have been shown to influence swash zone processes. Since typical wave runup
40 parameterizations do not account for these more complex processes, there is often significant scatter in
41 runup predictions when compared to observations (e.g., Atkinson et al., 2017; Stockdon et al., 2006).
42 Even flexible machine learning approaches based on extensive runup datasets or consensus-style ‘model
43 of models’ do not resolve prediction scatter in runup datasets (e.g., Atkinson et al., 2017; Passarella et al.,
44 2018b; Power et al., 2018). This suggests that the development of a perfect deterministic parameterization
45 of wave runup, especially with only reduced, easily obtainable inputs (i.e., wave height, wave period, and
46 beach slope), is improbable.

47

48 The resulting inadequacies of a single deterministic parameterization of wave runup can cascade up
49 through the scales to cause error in any larger model that uses a runup parameterization. It therefore makes
50 sense to clearly incorporate prediction uncertainty into wave runup predictions. In disciplines such as
51 hydrology and meteorology, with a more established tradition of forecasting, model uncertainty is often
52 captured by using ensembles (e.g., Bauer et al., 2015; Cloke and Pappenberger, 2009). The benefits of
53 ensemble modelling are typically superior skill and the explicit inclusion of uncertainty in predictions by
54 outputting a range of possible model outcomes. Commonly used methods of generating ensembles include

55 combining different models (Limber et al., 2018) or perturbing model parameters, initial conditions and/or
56 input data (e.g., via Monte Carlo simulations (e.g., Callaghan et al., 2013)).

57

58 An alternative approach to quantify prediction uncertainty is to incorporate scatter about a mean
59 prediction into model parameterizations. For example, wave runup predictions at every time step could
60 be modelled with a deterministic parameterization plus a noise component that captures the scatter about
61 the deterministic prediction caused by unresolved processes. If parameterizations are stochastic, or have
62 a stochastic component, repeated model runs (given identical initial and forcing conditions) produce
63 different model outputs – an ensemble – that represents a range of possible values the process could take.
64 This is broadly analogous to the method of “stochastic parameterization” used in the weather forecasting
65 community for sub-grid scale processes and parameterizations (Berner et al., 2017). In these applications,
66 stochastic parameterization has been shown to produce better predictions than traditional ensemble
67 methods and is now routinely used by many operational weather forecasting centers (Berner et al., 2017;
68 Buchanan, 2018).

69

70 Stochastically varying a deterministic wave runup parameterization to form an ensemble still requires
71 defining the stochastic term — i.e., the stochastic element that should be added to the predicted runup at
72 each model time step. An alternative to specifying a predefined distribution or a noise term added to a
73 parameterization is to learn and parameterize the variability in wave runup from observational data using
74 machine learning techniques. Machine learning has had a wide range of applications in coastal
75 morphodynamics research (Goldstein et al., 2018) and has shown specific utility in understanding swash
76 processes (Passarella et al., 2018b; Power et al., 2018) as well as storm driven erosion (Beuzen et al.,
77 2018; den Heijer et al., 2012; Goldstein and Moore, 2016; Palmsten et al., 2014; Plant and Stockdon,
78 2012). While many machine learning algorithms and applications are often used to optimize deterministic
79 predictions, a Gaussian process is a probabilistic machine learning technique that directly captures model
80 uncertainty from data (Rasmussen and Williams, 2006). Recent work has specifically used Gaussian
81 processes to model coastal processes such as large scale coastline erosion (Kupilik et al., 2018) and
82 estuarine hydrodynamics (Parker et al., 2019).

83

84 The work presented here is focused on using a Gaussian process to build a data-driven probabilistic
85 predictor of wave runup that includes estimates of uncertainty. While quantifying uncertainty in runup
86 predictions from data is useful in itself, the benefit of this methodology is in explicitly including the
87 uncertainty with the runup predictor in a larger model that uses a runup parametrization, such as a coastal
88 dune erosion model. Dunes on sandy coastlines provide a natural barrier to storm erosion by absorbing
89 the impact of incident waves and storm surge and helping to prevent or delay flooding of coastal
90 hinterland and infrastructure (Mull and Ruggiero, 2014; Sallenger, 2000; Stockdon et al., 2007). The
91 accurate prediction of coastal dune erosion is therefore critical for characterizing the vulnerability of dune
92 and beach systems and coastal infrastructure to storm events. A variety of methods are available for
93 modelling dune erosion including: simple conceptual models relating hydrodynamic forcing, antecedent
94 morphology and dune response (Sallenger, 2000); empirical dune-impact models that relate time-
95 dependent dune erosion to the force of wave impact at the dune (Erikson et al., 2007; Larson et al., 2004;
96 Palmsten and Holman, 2012); data-driven machine learning models (Plant and Stockdon, 2012); and more
97 complex physics-based models (Roelvink et al., 2009). In this study, we focus on dune-impact models,
98 which are simple, commonly used models that typically rely on a parameterization of wave runup to
99 model time-dependent dune erosion. As inadequacies in the runup parameterization can jeopardize the
100 success of model results (Overbeck et al., 2017; Palmsten and Holman, 2012; Splinter et al., 2018), it
101 makes sense to use a runup predictor that includes prediction uncertainty.

102

103 The overall aim of this work is to demonstrate how probabilistic data-driven methods can be used with
104 deterministic models to develop ensemble predictions, an idea that could be applied more generally to
105 other numerical models of geomorphic systems. **Sect. 2** first describes the Gaussian process model theory.
106 In **Sect. 3** the Gaussian process runup predictor is developed. In **Sect. 4** an example application of the
107 Gaussian process predictor of runup inside a morphodynamic model of coastal dune erosion to build a
108 ‘hybrid’ model (Goldstein and Coco, 2015; Krasnopolsky and Fox-Rabinovitz, 2006) that can generate
109 ensemble output is presented. A discussion of the results and technique is provided in **Sect. 5** followed

110 by conclusions in **Sect. 6**. The data and code used to develop the Gaussian process runup predictor in this
111 manuscript are publicly available at https://github.com/TomasBeuzen/BeuzenEtAl_GP_Paper.

112 2 Gaussian Processes

113 2.1 Gaussian Process Theory

114 Gaussian processes (GPs) are data-driven, non-parametric models. A brief introduction to GPs is given
115 here; for a more detailed introduction the reader is referred to Rasmussen and Williams (2006). There are
116 two main approaches to determine a function that best parameterizes a process over an input space: 1)
117 select a class of functions to consider, e.g., polynomial functions, and best fit the functions to the data (a
118 parametric approach); or, 2) consider all possible functions that could fit the data, and assign higher
119 weight to functions that are more likely (a non-parametric approach) (Rasmussen and Williams, 2006).
120 In the first approach it is necessary to decide on a class of functions to fit to the data – if all or parts of the
121 data are not well modelled by the selected functions, then the predictions may be poor. In the second
122 approach there is an infinite set of possible functions that could fit a data set (imagine the number of paths
123 that could be drawn between two points on a graph). A GP addresses the problem of infinite possible
124 functions by specifying a probability distribution over the space of possible functions that fit a given
125 dataset. Based on this distribution, the GP quantifies what function most likely fits the underlying process
126 generating the data and gives confidence intervals for this estimate. Additionally, random samples can
127 also be drawn from the distribution to provide examples of what different functions that fit the dataset
128 might look like.

129

130 A GP is defined as a collection of random variables, any finite set of which has a multivariate Gaussian
131 distribution. The random variables in a GP represent the value of the underlying function that describes
132 the data, $f(x)$, at location x . The typical workflow for a GP is to define a prior distribution over the space
133 of possible functions that fit the data, form a posterior distribution by conditioning the prior on observed
134 input/output data pairs (“training data”), and to then use this posterior distribution to predict unknown
135 outputs at other input values (“testing data”). The key to GP modelling is the use of the multivariate
136 Gaussian distribution, which has simple closed form solutions to the aforementioned conditioning
137 process, as described below.

138

139 Whereas a univariate Gaussian distribution is defined by a mean and variance (i.e., $\mathcal{N}(\mu, \sigma^2)$), a GP (a
140 multivariate Gaussian distribution) is completely defined by a mean function $m(\mathbf{x})$ and covariance
141 function $k(\mathbf{x}, \mathbf{x}')$ (also known as a “kernel”), and is typically denoted:

142

$$143 \quad f(\mathbf{x}) \sim \mathcal{N}(m(\mathbf{x}), k(\mathbf{x}, \mathbf{x}')) \quad (1)$$

144

145 Where \mathbf{x} is an input vector of dimension D ($\mathbf{x} \in \mathbb{R}^D$), and f is the unknown function describing the data.
146 Note that for the remainder of this paper, a variable denoted in bold text represents a vector. The mean
147 function, $m(\mathbf{x})$, describes the expected mean value of the function describing the data at location \mathbf{x} , while
148 the covariance function encodes the correlation between the function values at locations in \mathbf{x} .

149

150 These concepts of GP development are further described using a hypothetical dataset of significant wave
151 height (H_s) versus wave runup (R_2) shown in **Fig. 1A**. The first step of GP modelling is to constrain the
152 infinite set of functions that could fit a dataset by defining a prior distribution over the space of functions.
153 This prior distribution encodes belief about what the underlying function is expected to look like (e.g.,
154 smooth/erratic, cyclic/random, etc.) before constraining the model with any observed training data.
155 Typically it is assumed that the mean function of the GP prior, $m(\mathbf{x})$, is 0 everywhere, to simplify notation
156 and computation of the model (Rasmussen and Williams, 2006). Note that this does not limit the GP
157 posterior to be a constant mean process. The covariance function, $k(\mathbf{x}, \mathbf{x}')$, ultimately encodes what the
158 underlying functions look like because it controls how similar the function value at one input point is to
159 the function value at other input points.

160

161 There are many different types of covariance functions or “kernels”. One of the most common, and the
162 one used in this study, is the squared exponential covariance function:

163

$$164 \quad k(x_i, x_j) = \sigma_f^2 \exp\left[-\sum_{d=1}^D \frac{1}{2l_d^2} (x_{d,i} - x_{d,j})^2\right] \quad (2)$$

165

166 Where σ_f is the signal variance and l is known as the length-scale, both of which are hyperparameters in
 167 the model that can be estimated from data (discussed further in **Sect. 2.2**). Together the mean function
 168 and covariance function specify a multivariate Gaussian distribution:

169

$$170 \quad f(\mathbf{x}) \sim \mathcal{N}(\mathbf{0}, K) \quad (3)$$

171

172 Where f is the output of the prior distribution, the mean function is assumed to be $\mathbf{0}$ and K is the covariance
 173 matrix made by evaluating the covariance function at arbitrary input points that lie within the domain
 174 being modelled (i.e., $K(x, x)_{i,j} = k(x_i, x_j)$). Random sample functions can be drawn from this prior
 175 distribution as demonstrated in **Fig. 1B**.

176

177 The goal is to determine which of these functions actually fit the observed data points (training data) in
 178 **Fig. 1A**. This can be achieved by forming a posterior distribution on the function space by conditioning
 179 the prior with the training data. Roughly speaking, this operation is mathematically equivalent to drawing
 180 an infinite number of random functions from the multivariate Gaussian prior (**Eq. (3)**), and then rejecting
 181 those that do not agree with the training data. As mentioned above, the multivariate Gaussian offers a
 182 simple, closed form solution to this conditioning. Assuming that our observed training data is noiseless
 183 (i.e., y exactly represents the value of the underlying function f) then we can condition the prior
 184 distribution with the training data samples (\mathbf{x}, y) to define a posterior distribution of the function value (f^*)
 185 at arbitrary test inputs (\mathbf{x}^*) :

186

$$187 \quad f^* | \mathbf{y} \sim \mathcal{N}(K_* K^{-1} \mathbf{y}, K_{**} - K_* K^{-1} K_*^T) \quad (4)$$

188

189 Where f^* is the output of the posterior distribution at the desired test points \mathbf{x}^* , \mathbf{y} is the training data outputs
 190 at inputs \mathbf{x} , K_* is the covariance matrix made by evaluating the covariance function (**Eq. (2)**) between the
 191 test inputs \mathbf{x}^* and training inputs \mathbf{x} (i.e., $k(\mathbf{x}^*, \mathbf{x})$), K is the covariance matrix made by evaluating the
 192 covariance function between training data points \mathbf{x} , and K_{**} is the covariance matrix made by evaluating
 193 the covariance function between test points \mathbf{x}^* . Function values can be sampled from the posterior

194 distribution as shown in **Fig. 1C**. These samples represent random realizations of what the underlying
195 function describing the training data could look like.

196

197 As stated earlier, in **Eq. (4)** and **Fig. 1C** there is an assumption that the training data is noiseless and
198 represents the exact value of the function at the specific point in input space. In reality, there is error
199 associated with observations of physical systems, such that:

200

$$201 \mathbf{y} = f(\mathbf{x}) + \varepsilon \quad (5)$$

202

203 Where ε is assumed to be independent identically distributed Gaussian noise with variance σ_n^2 . This noise
204 can be incorporated into the GP modelling framework through the use of a white noise kernel that adds
205 an element of Gaussian white noise into the model:

206

$$207 k(x_i, x_j) = \sigma_n^2 \delta_{ij} \quad (6)$$

208

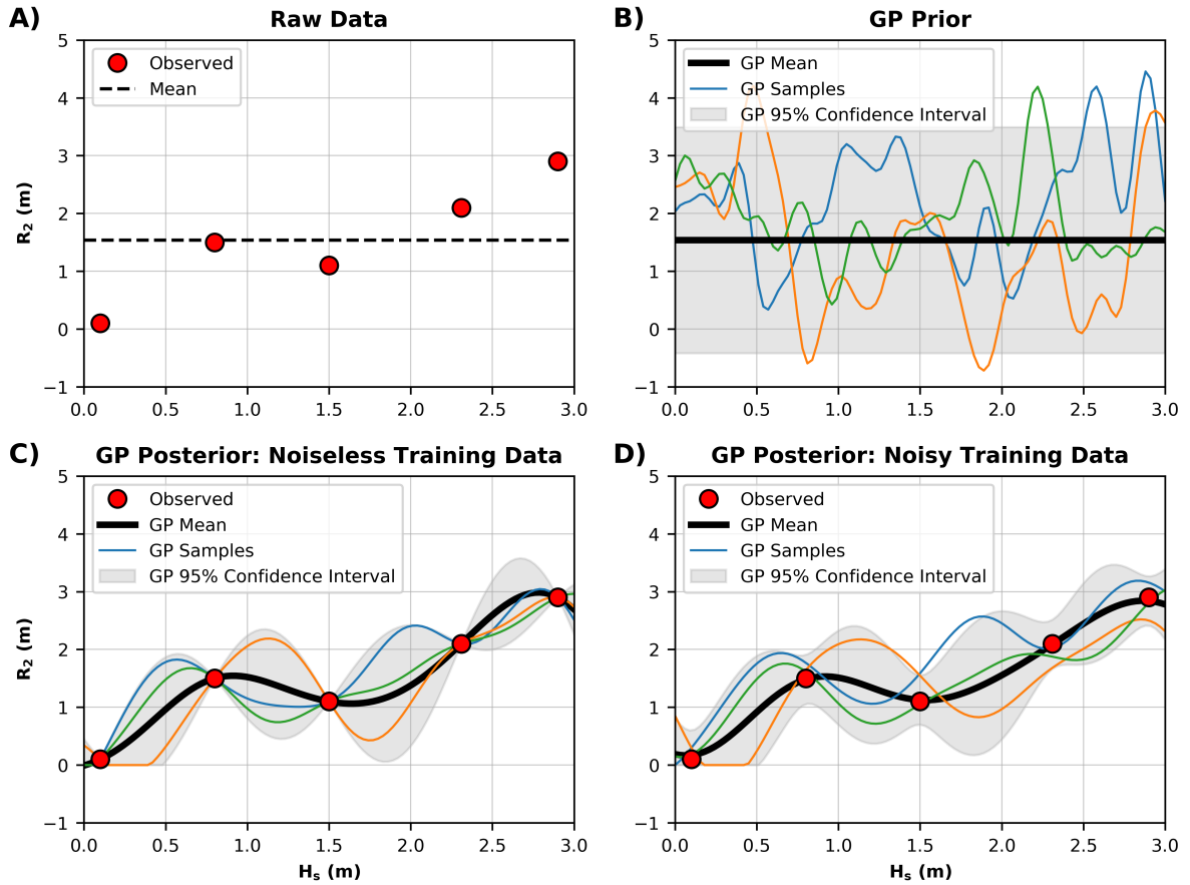
209 Where σ_n^2 is the variance of the noise and δ_{ij} is a Kronecker delta which is 1 if $i = j$ and 0 otherwise. The
210 squared exponential kernel and white noise kernel are closed under addition and product (Rasmussen and
211 Williams, 2006), such that they can simply be combined to form a custom kernel for use in the GP:

212

$$213 k(x_i, x_j) = \sigma_f^2 \exp \left\{ - \sum_{d=1}^D \frac{1}{2l_d^2} (x_{d,i} - x_{d,j})^2 \right\} + \sigma_n^2 \delta_{ij} \quad (7)$$

214

215 The combination of kernels to model different signals in a dataset (that vary over different spatial or
216 temporal timescales) is common in applications of GPs (Rasmussen and Williams, 2006; Reggente et al.,
217 2014; Roberts et al., 2013). Samples drawn from the resultant “noisy” posterior distribution are shown
218 in **Fig. 1D** in which the GP can now be seen to not fit the observed training data precisely.



219

220 Fig. 1: A) Five hypothetical random observations of significant wave height (H_s) and 2% wave runup elevation (R_2). B) The Gaussian
 221 process (GP) prior distribution. C) The GP posterior distribution, formed by conditioning the prior distribution in (B) with the
 222 observed data points in (A), assuming the observations are noise-free. D). The GP posterior distribution conditioned on the
 223 observations with a noise component.

224

225 2.2 Gaussian Process Kernel Optimization

226 In Eq. (7) there are three hyperparameters: the signal variance (σ_f), the length scale (l) and the noise
 227 variance (σ_n). These hyperparameters are typically unknown but can be estimated and optimized based
 228 on the particular dataset. Here, this optimization is performed by using the typical methodology of
 229 maximizing the log-marginal-likelihood of the observed data y given the hyperparameters:

230

$$231 \log p(y|x, \sigma_f, l, \sigma_n)$$

(8)

232

233 The Python toolkit SciKit-Learn (Pedregosa et al., 2011) was used to develop the GP described in this
234 study. For the Reader unfamiliar with the Python programming language, alternative programs for
235 developing Gaussian Processes include Matlab (Rasmussen and Nickisch, 2010) and R (Dancik and
236 Dorman, 2008; MacDonald et al., 2015).

237 **2.3 Training a Gaussian Process Model**

238 It is standard practice in the development of data-driven machine learning models to divide the available
239 dataset into training, validation and testing subsets. The training data is used to fit model parameters. The
240 validation data is used to evaluate model performance and the model hyperparameters are usually varied
241 until performance on the validation data is optimized. Once the model is optimized, the remaining test
242 dataset is used to objectively evaluate its performance and generalizability. A decision must be made
243 about how to split a dataset into training, validation and testing subsets. There are many different
244 approaches to handle this splitting process; for example, random selection, cross-validation, stratified
245 sampling, or a number of other deterministic sampling techniques (Camus et al., 2011). The exact
246 technique used to generate the data subsets often depends on the problem at hand. Here, there were two
247 constraints to be considered; first, the computational expense of GPs scales by $O(n^3)$ (Rasmussen and
248 Williams, 2006), so it is desirable to keep the training set as small as possible without deteriorating model
249 performance; and, secondly, machine learning models typically perform poorly with out-of-sample
250 predictions (i.e., extrapolation), so it is desirable to include in the training set the data samples that
251 captures the full range of variability in the data. Based on these constraints, we used a maximum
252 dissimilarity algorithm (MDA) to divide the available data into training, validation and testing sets.

253

254 The MDA is a deterministic routine that iteratively adds a data point to the training set based on how
255 dissimilar it is to the data already included in the training set. Camus et al. (2011) provide a comprehensive
256 introduction to the MDA selection routine and it has been previously used in machine learning studies
257 (e.g., Goldstein et al., 2013). Briefly, to initialize the MDA routine, the data point with the maximum sum
258 of dissimilarity (defined by Euclidean distance) to all other data points is selected as the first data point

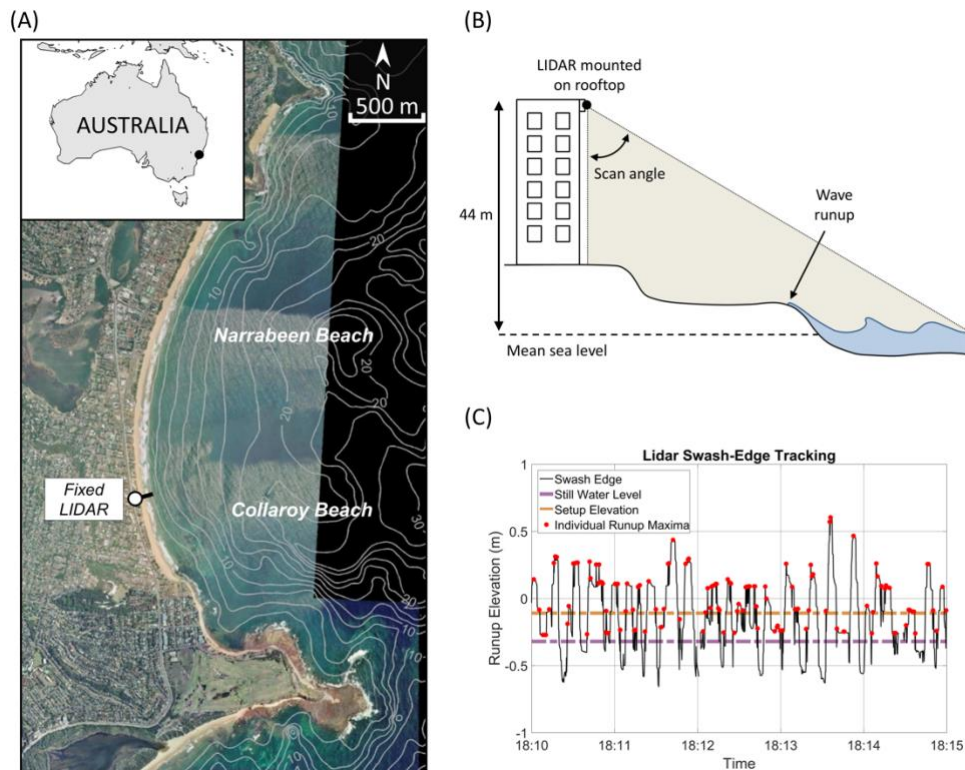
259 to be added to the training data set. Additional data points are included in the training set through an
260 iterative process whereby the next data point added is the one with maximum dissimilarity to those already
261 in the training set - this process continues until a user-defined training set size is reached. In this way the
262 MDA routine produces a set of training data that captures the range of variability present in the full
263 dataset. The data not selected for the training set are equally and randomly split to form the validation
264 dataset and test dataset. While alternative data-splitting routines are available, including simple random
265 sampling, stratified random sampling, self-organizing maps and k-means clustering (Camus et al., 2011),
266 the MDA routine used in this study was found in preliminary testing (not presented) to produce the best
267 GP performance with the least computational expense.

268 3 Development of a Gaussian Process Runup Model

269 3.1 Runup Data

270 In 2014, an extended-range LIDAR (Light Detection And Ranging) device (SICK LD-LRS 2110) was
271 permanently installed on the rooftop of a beachside building (44 m above mean sea level) at Narrabeen-
272 Collaroy Beach (hereafter referred to simply as Narrabeen) on the south-east coast of Australia (**Fig. 2**).
273 Since 2014, this LIDAR has continuously scanned a single cross-shore profile transect extending from
274 the base of the beachside building to a range of 130 m, capturing the surface of the beach profile and
275 incident wave swash at a frequency of 5 Hz in both daylight and non-daylight hours. Specific details of
276 the LIDAR setup and functioning can be found in (Phillips et al., 2019).

277
278



279

280 **Fig. 2:** A) Narrabeen Beach, located on the southeast coast of Australia. B) Conceptual figure of the fixed LIDAR setup. C) A five-
281 minute extract of runup elevation extracted from the LIDAR data, individual runup maxima are marked with red circles.

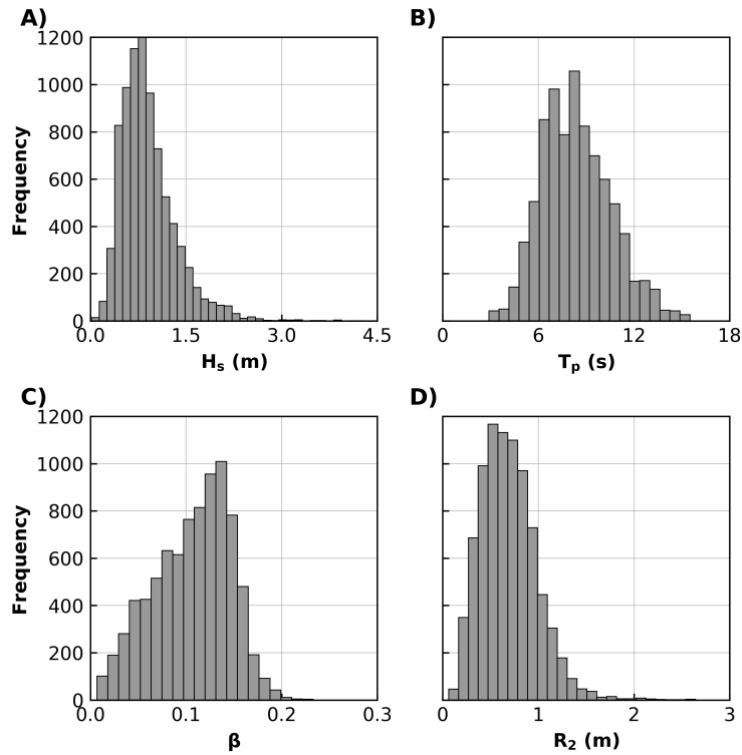
282

283 Narrabeen Beach is a 3.6 km long embayed beach bounded by rocky headlands. It is composed of fine to
284 medium quartz sand ($D_{50} \approx 0.3$ mm), with a $\sim 30\%$ carbonate fraction. Offshore, the coastline has a steep
285 and narrow (20 – 70 km) continental shelf (Short and Trenaman, 1992). The region is microtidal and
286 semidiurnal with a mean spring tidal range of 1.6 m and has a moderate to high energy deep water wave
287 climate characterized by persistent long-period south-southeast swell waves that is interrupted by storm
288 events (significant wave height > 3 m) typically 10 – 20 times per year (Short and Trenaman, 1992). In
289 the present study, approximately one year of the high-resolution wave runup LIDAR dataset available at
290 Narrabeen is used to develop a data-driven parameterization of the 2% exceedance of wave runup (R_2).
291 Data used to develop this parameterization were at hourly resolution and include: R_2 , the beach slope (β),
292 offshore significant wave height (H_s), and peak wave period (T_p). These data are described below and
293 have been commonly used to parameterize R_2 in other empirical models of wave runup (e.g., Holman,
294 1986; Hunt, 1959; Stockdon et al., 2006).

295

296 Individual wave runup elevation on the beach profile was extracted on a wave-by-wave basis from the
297 LIDAR dataset (**Fig. 2C**) using the neural network runup detection tool developed by Simmons et al.
298 (2019). Hourly R_2 was calculated as the 2% exceedance value for a given hour of wave runup
299 observations. β was calculated as the linear (best-fit) slope of the beach profile over which two standard
300 deviations of wave runup values were observed during the hour. Hourly H_s and T_p data were obtained
301 from the Sydney Wave Rider buoy, situated 11 km offshore of Narrabeen in ~ 80 m water depth.
302 Narrabeen is an embayed beach, where prominent rocky headlands both attenuate and refract incident
303 waves. To remove these effects in the wave data and to emulate an open coastline and generalize the
304 parameterization of R_2 presented in this study, offshore wave data were first transformed to a nearshore
305 equivalent (10 m water depth) using a pre-calculated look-up table generated with the SWAN spectral
306 wave model based on a 10 m resolution grid (Booij et al., 1999), and then reverse shoaled back to deep
307 water wave data. A total of 8328 hourly samples of R_2 , β , H_s and T_p were extracted to develop a
308 parameterization of R_2 in this study. Histograms of this data are shown in **Fig. 3**.

309



310

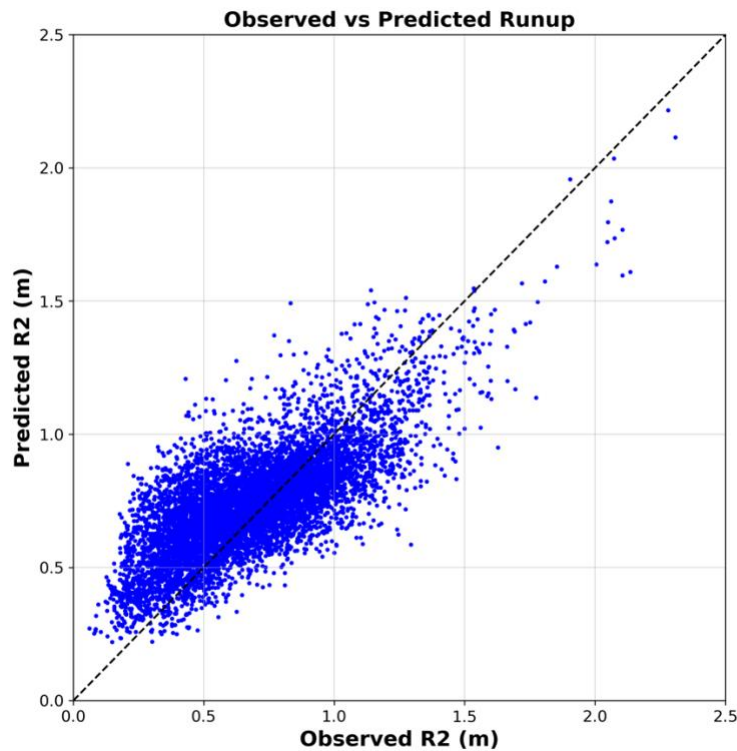
311 **Fig. 3:** Histograms of the 8328 data samples extracted from the Narrabeen LIDAR: (A) significant wave height (H_s); (B) peak wave
 312 period (T_p); (C) beach slope (β); and, (D) 2% wave runup elevation (R_2).

313 3.2 Training Data for the GP Runup Predictor

314 To determine the optimum training set size, kernel and model hyperparameters, a number of different
 315 user-defined training set sizes were trialed using the MDA selection routine discussed in **Sect. 2.3**. The
 316 GP was trained using different amounts of data and hyperparameters were optimized on the validation
 317 data set only. It was found that a training set size of only 5% of the available dataset (training dataset =
 318 416 of 8328 available samples, validation dataset = 3956 samples, testing dataset = 3956 samples) was
 319 required to develop an optimum GP model. Training data sizes beyond this value produced negligible
 320 changes in GP performance but considerable increases in computational demand, similar to findings of
 321 previous work (Goldstein and Coco, 2014; Tinoco et al., 2015). Results presented below discuss the
 322 performance of the GP on the testing dataset which was not used in GP training or validation.

323 3.3 Runup Predictor Results

324 Results of the GP R_2 predictor on the 3956 test samples are shown in **Fig. 4**. This figure plots the mean
325 GP predictions against corresponding observations of R_2 . The mean GP prediction performs well on the
326 test data, with a root-mean-squared-error (RMSE) of 0.18 m and bias (B) of 0.02 m. For comparison, the
327 commonly used R_2 parameterization of Stockdon et al. (2006) tested on the same data has a RMSE of
328 0.36 m and B of 0.21 m. Despite the relatively accurate performance of the GP on this dataset, there
329 remains significant scatter in the observed versus predicted R_2 in **Fig. 4**. This is consistent with recent
330 work by Atkinson et al. (2017) showing that commonly used predictors of R_2 always result in scatter.
331



332

333 **Fig. 4: Observed 2% wave runup (R_2) versus the R_2 predicted by the Gaussian process model. Root-mean-squared-error (RMSE) is**
334 **0.36 m, bias (B) is 0.02 m and squared correlation (r^2) is 0.54.**

335

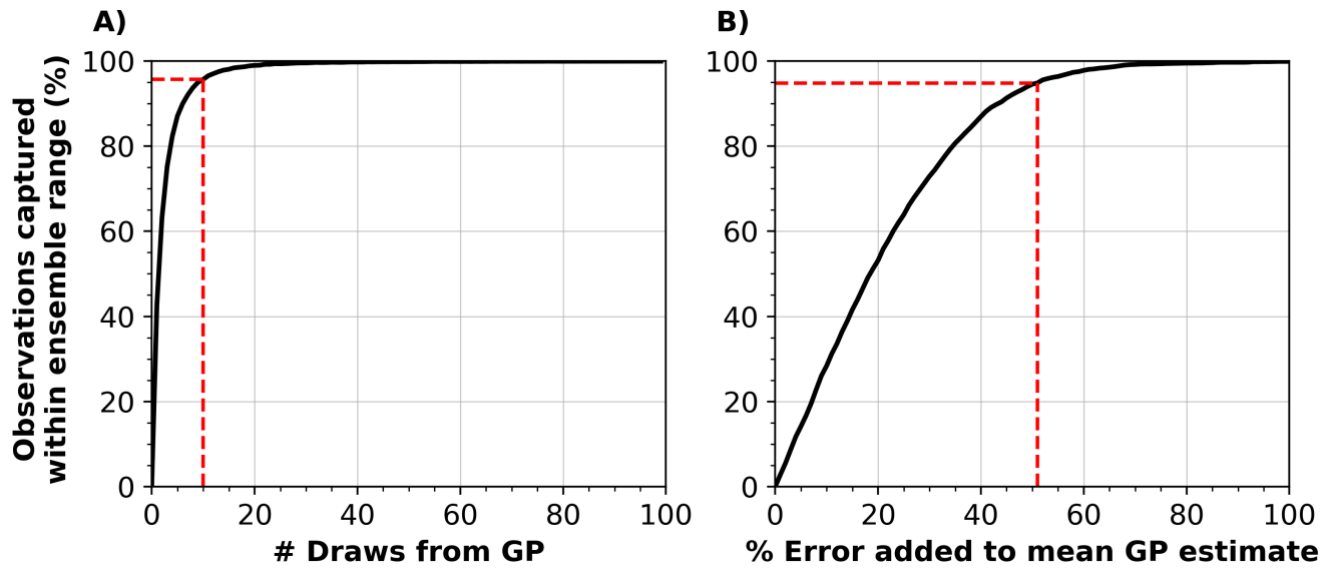
336 **As discussed in Sect. 1 scatter in runup predictions is likely a result of unresolved processes in the model**
337 **such as wave dispersion, wave spectrum, nearshore morphology or a range of other possible processes.**

338 **Regardless of the origin,** here this scatter (uncertainty) is used to form ensemble predictions. The GP

339 developed here not only gives a mean prediction as used in **Fig. 4**, but it specifies a multivariate Gaussian
340 distribution from which different random functions that describe the data can be sampled. Random
341 samples of wave runup from the GP can capture uncertainty around the mean runup prediction (as was
342 demonstrated in the hypothetical example in **Fig. 1D**). To assess how well the GP model captures
343 uncertainty, random samples are successively drawn from the GP and the number of R_2 measurements
344 captured with each new draw are determined. Only 10 random samples drawn from the GP are required
345 to capture 95% of the scatter in R_2 (**Fig. 5A**). This process of drawing random samples from the GP was
346 repeated 100 times with results showing that the above is true for any 10 random samples, with an average
347 capture percentage of 95.7% and range of 94.9% to 96.1% for 10 samples across the 100 trials. As a point
348 of contrast, **Fig. 5B** shows how much arbitrary error would need to be added to the mean R_2 prediction to
349 capture scatter about the mean to emulate the uncertainty captured by the GP. It can be seen that the mean
350 R_2 prediction would need to vary by $\pm 51\%$ to capture 95% of the scatter present in the runup data. This
351 demonstrates how random models of runup drawn from the GP effectively capture uncertainty in R_2
352 predictions. These randomly drawn R_2 models can be used within a larger dune-impact model to produce
353 an ensemble of dune erosion predictions that includes uncertainty in runup predictions, as demonstrated
354 in **Sect. 4**.

355

356



357

358 Fig. 5: A) Percent of observed runup values captured within the range of ensemble predictions made by randomly sampling different
 359 runup values from the Gaussian process. Only 10 randomly drawn models can form an ensemble that captures 95% of the scatter
 360 in observed R_2 values. B) An experiment showing how much arbitrary error would need to be added to the mean GP runup
 361 prediction in order to capture scatter in R_2 observations. The mean GP prediction would have to vary by 51% in order to capture
 362 95% of scatter in R_2 observations.

363 4 Application of a Gaussian Process Runup Predictor in a Coastal Dune Erosion Model

364 4.1 Dune Erosion Model

365 We use the dune erosion model of Larson et al. (2004) as an example of how the GP runup predictor can
366 be used to create an ensemble of dune erosion predictions, and thus provide probabilistic outcomes with
367 uncertainty bands needed in coastal management. The dune erosion model is subsequently referred to as
368 LEH04 and is defined as follows:

369

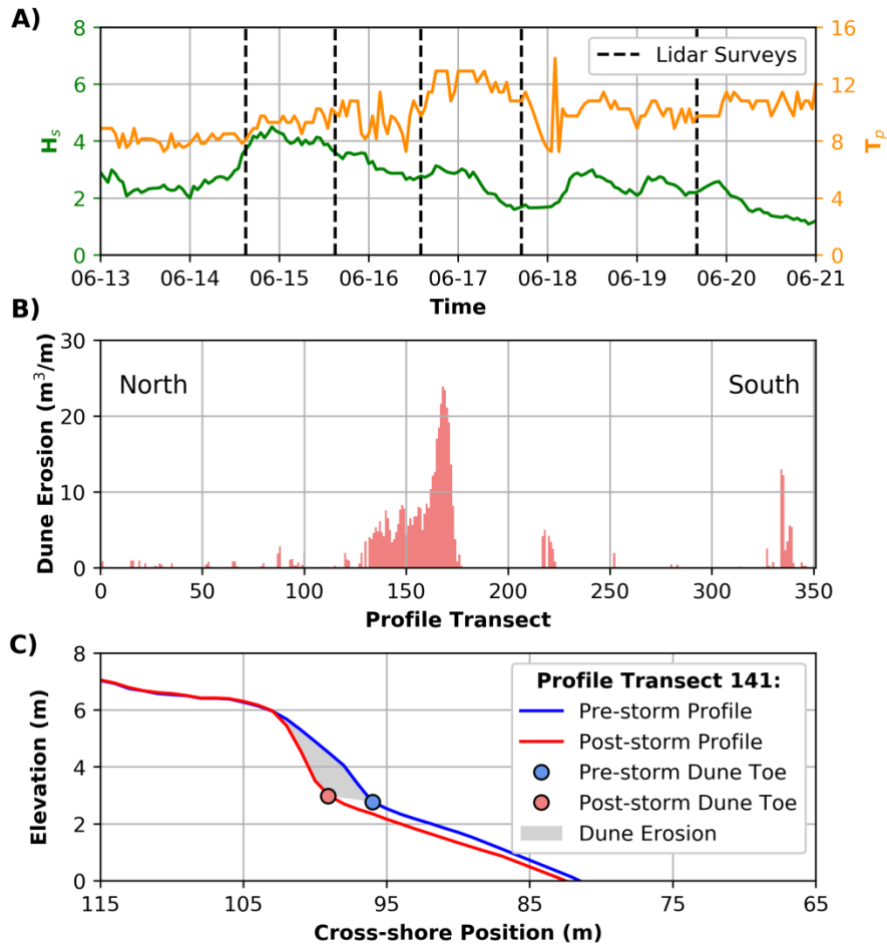
$$370 \quad dV = 4C_s(R_2 - z_b)^2\left(\frac{t}{T}\right) \quad (9)$$

371

372 Where dV (m^3/m) is the volumetric dune erosion per unit width alongshore for a given time step t , z_b (m)
373 is the time-varying dune toe elevation, T (s) is the wave period for that time step, R_2 (m) is the 2% runup
374 exceedance for that time step, and C_s is the transport coefficient. Note that the original equation used a
375 best-fit relationship to define the runup term, R (see Eq. (36) in Larson et al., 2004) rather than R_2 .
376 Subsequent modifications of the LEH04 model have been made to adjust the collision frequency (i.e. the
377 t/T term; e.g., Palmsten and Holman (2012), Splinter and Palmsten (2012)), however we retain the model
378 presented in **Eq. (9)** for the purpose of providing a simple illustrative example. At each time step, dune
379 volume is eroded in bulk and the dune toe is adjusted along a predefined slope (defined here as the linear
380 slope between the pre- and post-storm dune toe) so that erosion causes the dune toe to increase in elevation
381 and recede landward. Dune erosion and dune toe recession only occurs when wave runup (R_2) exceeds
382 the dune toe (i.e., $R_2 - z_b > 0$) and cannot progress vertically beyond the maximum runup elevation. When
383 R_2 does not exceed z_b , $dV = 0$. The GP R_2 predictor described in **Sect. 3** is used to stochastically
384 parameterize wave runup in the LEH04 model and form ensembles of dune erosion predictions. The
385 model is applied to new data not used to train the GP R_2 predictor, using detailed observations of dune
386 erosion caused by a large coastal storm event at Narrabeen Beach, southeast Australia in 2011.

387 4.2 June 2011 Storm Data

388 In June 2011 a large coastal storm event impacted the southeast coast of Australia. This event resulted in
389 variable alongshore dune erosion at Narrabeen Beach, which was precisely captured by airborne LIDAR
390 immediately pre-, during, and post-storm by five surveys conducted approximately 24 hours apart. Cross-
391 shore profiles were extracted from the Lidar data at 10 m alongshore intervals as described in detail in
392 Splinter et al. (2018), resulting in 351 individual profiles (**Fig. 6**). The June 2011 storm lasted 120 hours.
393 Hourly wave data was recorded by the Sydney wave rider buoy located in ~80 m water depth directly to
394 the southeast of Narrabeen Beach. As with the hourly wave data used to develop the GP model of R_2
395 (**Sect. 3.1**), hourly wave data for each of the 351 profiles for the June 2011 storm was obtained by first
396 transforming offshore wave data to the nearshore equivalent at 10 m water depth directly offshore of each
397 profile using the SWAN spectral wave model (Booij et al., 1999), and then reverse shoaling back to
398 equivalent deep water wave data, to account for the effects of wave refraction and attenuation caused by
399 the distinctly curved Narrabeen embayment. The tidal range during the storm event was measured in-situ
400 at the Fort Denison Tide Gauge (located within Sydney Harbour approximately 16 km south of
401 Narrabeen) as 1.58 m (mean spring tidal range at Narrabeen is 1.6 m). **As can be seen in Fig. 6 the wave**
402 **conditions for the June 2011 storm lie within the range of the training dataset used to develop the GP**
403 **runup predictor.** The hydrodynamic time series and airborne LIDAR observations of dune change are
404 used to demonstrate how the LEH04 model can be used with the GP predictor of runup to generate
405 stochastic parameterizations and create probabilistic model ensembles (**Eq. (9)**).



406

407 Fig. 6: June 2011 storm data. A) Offshore H_s and T_p with vertical dashed lines indicating the time of the LIDAR surveys, B) Measured
 408 (pre vs post storm) dune erosion volumes for the 351 profile transects extracted from LIDAR data, C) Example pre- (blue) and post-
 409 storm (red) profile cross sections showing dune toes (coloured circles) and dune erosion volume (grey shading).

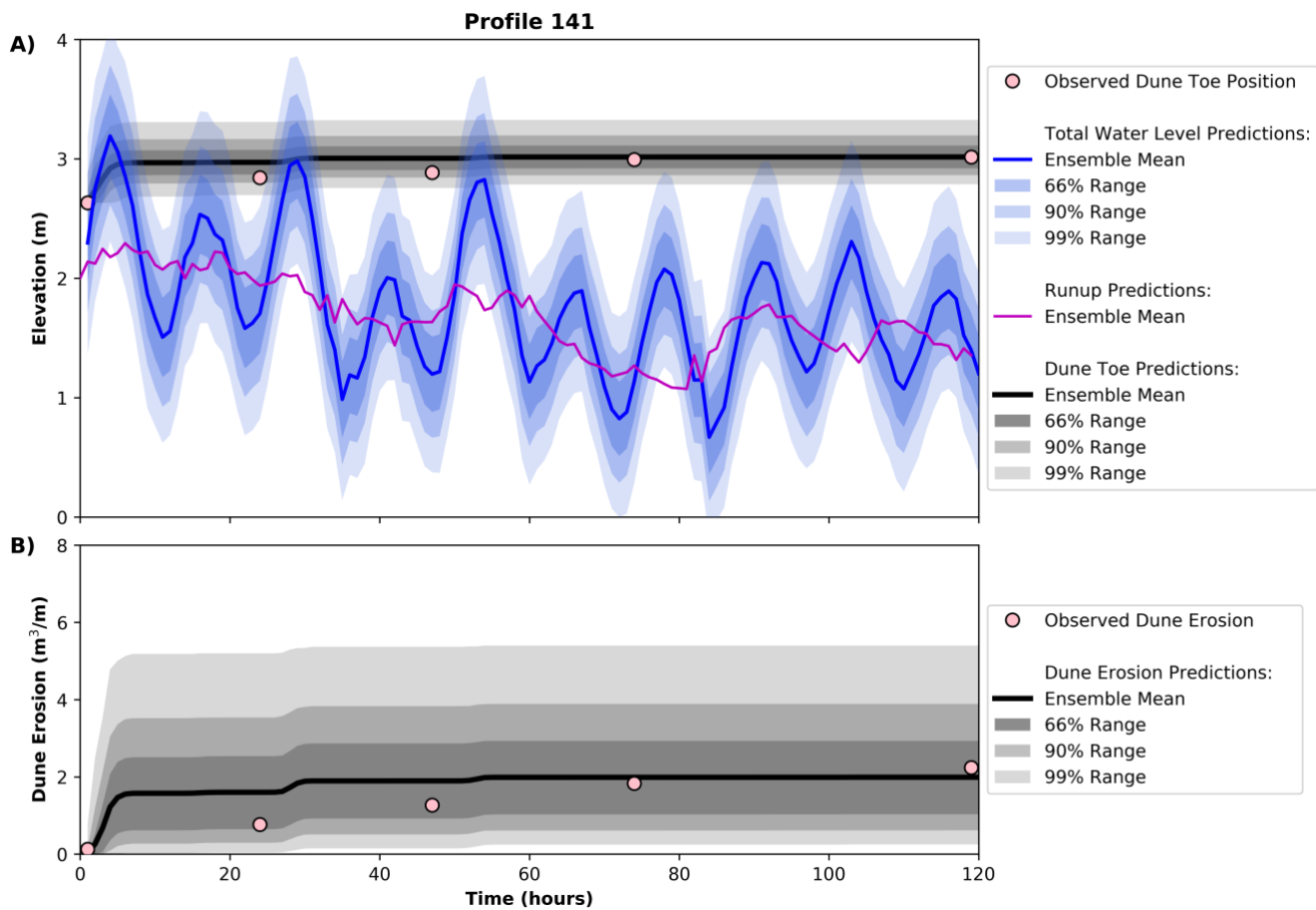
410 For each of the 351 available profiles, the pre-, during and post-storm dune toe positions were defined as
 411 the local maxima of curvature of the beach profile following the method of Stockdon et al. (2007). Dune
 412 erosion at each profile was then defined as the difference in subaerial beach volume landward of the pre-
 413 storm dune toe, as shown in **Fig. 6C**. Of the 351 profiles, only 117 had storm driven dune erosion (**Fig.**
 414 **6B**). For the example demonstration presented here, only profiles for which the post-storm dune toe
 415 elevation was at the same or higher elevation than the pre-storm dune toe are considered; which is a basic
 416 assumption of the LEH04 model. Of the 117 profiles with storm erosion, 40 profiles met these criteria.

417 For each of these profiles, the linear slope between the pre- and post-storm dune toe was used to project
418 the dune erosion calculated using the LEH04 model.

419

420 The LEH04 dune erosion model (**Eq. (9)**) has a single tuneable parameter, the transport coefficient C_s .
421 There is ambiguity in the literature regarding the value of C_s . Larson et al. (2004) developed an empirical
422 equation to relate C_s to wave height (H_{rms}) and grain size (D_{50}) using experimental data. Values ranged
423 from 1×10^{-5} to 1×10^{-1} , and Larson et al. (2004) used 1.7×10^{-4} based on field data from Birkemeier et
424 al. (1988). Palmsten and Holman (2012) used LEH04 to model dune erosion observed in a large wave
425 tank experiment conducted at the O.H. Hinsdale Wave Research Laboratory at Oregon State University.
426 The model was shown to accurately reproduce dune erosion when applied in hourly time steps using a C_s
427 of 1.34×10^{-3} , based on the empirical equation determined by Larson et al. (2004). Mull and Ruggiero
428 (2014) used values of 1.7×10^{-4} and 1.34×10^{-3} as lower and upper bounds of C_s to model dune erosion
429 caused by a large storm event on the Pacific Northwest Coast of the USA and the laboratory experiment
430 used by Palmsten and Holman (2012). For the dune erosion experiment, the value of 1.7×10^{-4} was found
431 to predict dune erosion volumes closest to the observed erosion when applied in a single time step, with
432 an optimum value of 2.98×10^{-4} . Splinter and Palmsten (2012) found a best fit C_s of 4×10^{-5} in an
433 application to modelling dune erosion caused by a large storm event that occurred on the Gold Coast,
434 Australia. Ranasinghe et al. (2012) found a C_s value of 1.5×10^{-3} in an application at Narrabeen Beach,
435 Australia. It is noted that C_s values in these studies are influenced by the time step used in the model and
436 the exact definition of wave runup, R , used (Larson et al., 2004; Mull and Ruggiero, 2014; Palmsten and
437 Holman, 2012; Splinter and Palmsten, 2012). In practice, C_s could be optimized to fit any particular
438 dataset. However, for predictive applications the optimum C_s value may not be known in advance, since
439 it is unclear if subsequent storms at a given location will be well predicted using previously optimized C_s
440 values. A key goal of this work is to determine if using stochastic parameterizations to generate
441 ensembles that predict a range of dune erosion (based on uncertainty in the runup parameterization) can
442 still capture observed dune erosion even if the optimum C_s value is not known in advance. As such, a C_s
443 value of 1.5×10^{-3} is used in this example application based on previous work at Narrabeen Beach by

444 Ranasinghe et al. (2012). Sensitivity of model results to the choice of C_s are further discussed in **Sect.**
445 **4.3.**
446
447 An example at a single profile (profile 141, located approximately half-way up the Narrabeen embayment
448 as shown in **Fig. 6B**) of time-varying ensemble dune erosion predictions is provided in **Fig. 7**. It was
449 previously shown in **Fig. 5** that only 10 random samples drawn from the GP R_2 predictor were required
450 to capture 95% of the scatter in the R_2 data used to develop and test the GP. However, it is trivial to draw
451 many more samples than this from the GP - for example, drawing 10,000 samples takes less than one
452 second on a standard desktop computer. Therefore, to explore a large range of possible runup scenarios
453 during the 120-hour storm event, 10,000 different runup time series are drawn from the GP and used to
454 run LEH04 at hourly intervals, thus producing 10,000 model results of dune erosion. The effect of using
455 different ensemble sizes is explored in **Sect. 4.3**. **Fig. 7A** shows the time-varying distribution of the runup
456 models (blue) used to force LEH04 along with the time-varying prediction distribution of dune toe
457 elevations (grey) throughout the 120-hour storm event. To interpret model output probabilistically, the
458 mean of the ensemble is plotted, along with intervals capturing 66%, 90%, and 99% of the ensemble
459 output. These intervals are consistent with those used in IPCC for climate change predictions
460 (Mastrandrea et al., 2010) and in the context of the model results presented here, they represent varying
461 levels of confidence in the model output. For example, there is high confidence that the real dune erosion
462 will fall within the 66% ensemble prediction range. **Fig. 7B** shows the time-varying predicted distribution
463 of dune erosion volumes from the 10,000 LEH04 runs. It can be seen that while the mean value of the
464 ensemble predictions deviates slightly from the observed dune erosion, the observed erosion is still
465 captured well within the 66% envelope of predictions.



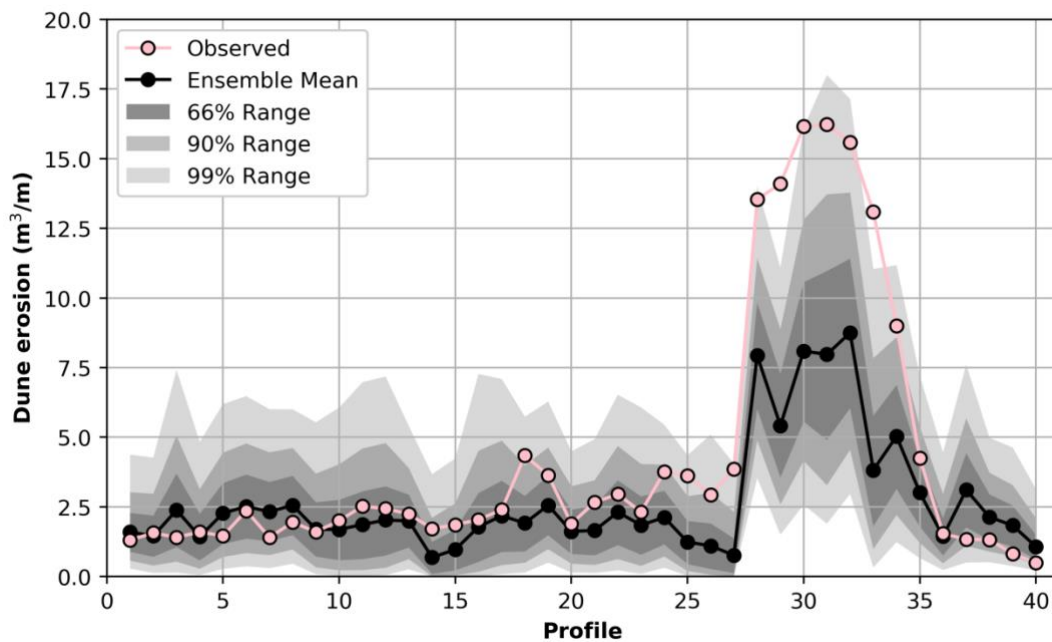
466

467 **Fig. 7:** Example of LEH04 used with the Gaussian process R_2 predictor to form an ensemble of dune erosion predictions. 10,000
 468 runup models are drawn from the Gaussian process and used to force the LEH04 model. A) **Total water level (measured water level**
 469 **+ R_2 ; blue)** and dune toe elevation (grey) for the 120-hour storm event. Bold colored line is the mean of the ensemble and shaded
 470 areas represent the regions captured by 66%, 90% and 99% of the ensemble predictions. **An example of just the R_2 prediction (no**
 471 **measured water level) from the Gaussian process is shown in the magenta line.** Pink dots denote the observed dune toe elevation
 472 throughout the storm event. B) The corresponding ensemble of dune erosion predictions.

473 Pre- and post-storm dune erosion results for the 40 profiles using 10,000 ensemble members and C_s of
 474 1.5×10^{-3} are shown in **Fig. 8**. The squared-correlation (r^2) for the observed and predicted dune erosion
 475 volumes is 0.85. Many of the profiles experienced only minor dune erosion ($< 2.5 \text{ m}^3/\text{m}$) and can be seen
 476 to be well predicted by the mean of the ensemble predictions. In contrast, the ensemble mean can be seen
 477 to under-predict dune erosion at profiles where high erosion volumes were observed (**profiles 29 – 34 in**
 478 **Fig. 8**), with some profiles not even captured by the uncertainty of the ensemble. However, the ensemble
 479 range of predictions for these **particular** profiles also has a large spread, indicative of high uncertainty in

480 predictions and the potential for high erosion to occur. It should be noted that the results presented in Fig.
 481 8 are based on an assumed (i.e., non-optimized) C_s value of 1.5×10^{-3} . Better prediction of large erosion
 482 events could potentially be achieved by increasing C_s or giving greater weighting to these events during
 483 calibration, but at the cost of over-predicting the smaller events. The exact effect of varying C_s is
 484 quantified in Sect. 4.3. Importantly, Fig. 8 demonstrates that even with a non-optimized C_s , uncertainty
 485 in the GP predictions can provide useful information about the potential for dune erosion, even if the
 486 mean dune erosion prediction deviates from the observation; a key advantage of the GP approach over a
 487 deterministic approach.

488



489

490 Fig. 8: Observed (pink dots) and predicted (black dots) dune erosion volumes for the 40 modelled profiles, using 10,000 runup models
 491 drawn from the Gaussian process and used to force the LEH04 model. Note that the 40 profiles shown are not uniformly spaced
 492 along the 3.5 km Narrabeen embayment. The black dots represent the ensemble mean prediction for each profile, while the shaded
 493 areas represent the regions captured by 66%, 90% and 99% of the ensemble predictions.

494 4.3 The Effect of C_s and Ensemble Size on Dune Erosion

495 In Sect. 4.2, the application of the GP runup predictor within the LEH04 model to produce an ensemble
 496 of dune erosion predictions was based on 10,000 ensemble members and a C_s value of 1.5×10^{-3} . The

497 sensitivity of results to the number of members in the ensemble and the value of the tunable parameter C_s ,
498 in Eq. (9) is presented in Fig. 9. The mean absolute error (MAE) between the mean ensemble dune erosion
499 predictions and the observed dune erosion, averaged across all 40 profiles, varies for R_2 ensembles of 5,
500 10, 20, 100, 1000, and 10,000 members and C_s values ranging from 10^{-5} to 10^{-1} (Fig. 9). As can be seen
501 in Fig. 9A and summarized in Table 1, the lowest MAE for the differing ensemble sizes is similar, ranging
502 from 1.50 to 1.64 m^3/m , suggesting that the number of ensemble members does not have a significant
503 impact on the resultant mean prediction. The lowest MAE for the different ensemble sizes corresponds to
504 C_s values between 2.8×10^{-3} (10,000 ensemble members) and 4.1×10^{-3} (5 ensemble members);
505 reasonably consistent with the value of 1.5×10^{-3} previously reported by Ranasinghe et al. (2012) for
506 Narrabeen Beach and within the range of C_s values presented in Larson et al. (2004).

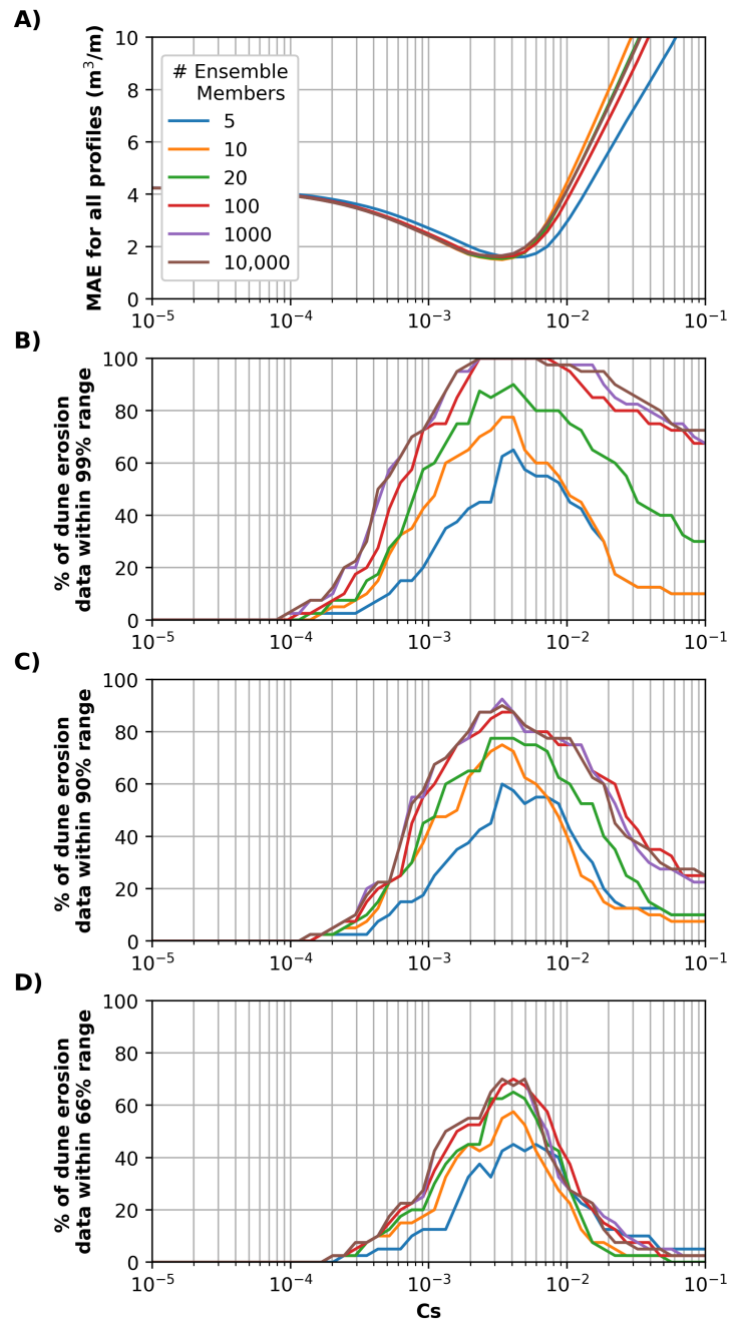
507

508 The key utility to using a data-driven GP predictor to produce ensembles is that a range of predictions at
509 every location is provided as opposed to a single erosion volume. The ensemble range provides an
510 indication of uncertainty in predictions, which can be highly useful for coastal engineers and managers
511 taking a risk-based approach to coastal hazard management. Fig. 9B-D displays the percentage of dune
512 erosion observations from the 40 profiles captured within ensemble predictions for C_s values ranging
513 from 10^{-5} to 10^{-1} . It can be seen that a high proportion of dune erosion observations are captured within
514 the 66%, 90% and 99% ensemble envelope across several orders of magnitude C_s . While the main purpose
515 of using ensemble runup predictions within LEH04 is to incorporate uncertainty in the runup prediction,
516 this result demonstrates that the ensemble approach is less sensitive to the choice of C_s than a deterministic
517 model and so can be useful for forecasting with non-optimized model parameters.

518

519 Results in Fig. 9 and Table 1 demonstrate that there is relatively little difference in model performance
520 when more than 10 to 100 ensemble members are used; consistent with results presented previously in
521 Fig. 5 that showed that only 10 random samples drawn from the GP R_2 predictor were required to capture
522 95% of the scatter in the R_2 data used to develop and test the GP. This suggests that the GP approach
523 efficiently captures scatter (uncertainty) in runup predictions and subsequently, dune erosion predictions,
524 requiring on the order of 10 samples; significantly less than the $10^3 - 10^6$ runs typically used in Monte

525 Carlo simulations to develop probabilistic predictions (e.g., Callaghan et al., 2008; Li et al., 2013;
526 Ranasinghe et al., 2012).



527
528 Fig. 9: Results of the stochastic parameterization methodology for R_2 ensembles of 5, 10, 20, 100, 1000, and 10,000 members and C_s
529 values ranging from 10^{-5} to 10^{-1} . A) The mean absolute error (MAE) between the median ensemble dune erosion predictions and the
530 observed dune erosion averaged across all 40 profiles. B), C) and D) show the percentage of dune erosion observations that fall
531 within the 99%, 90% and 66% ensemble prediction ranges respectively.

532 Table 1: Quantitative summary of Fig. 9, showing the optimum C_s value for differing ensemble sizes, along with the associated mean-
 533 absolute-error (MAE) and percent of the 40 dune erosion observations captured by the 66%, 90% and 99% ensemble prediction
 534 range.

Ensemble Members	Optimum C_s	MAE (m³/m)	r^2	Percent Captured in 66% Ensemble Range (%)	Percent Captured in 90% Ensemble Range (%)	Percent Captured in 99% Ensemble Range (%)
5	4.1×10^{-3}	1.59	0.86	45	57	65
10	3.4×10^{-3}	1.50	0.87	55	75	78
20	3.4×10^{-3}	1.54	0.86	62	78	88
100	3.3×10^{-3}	1.61	0.86	68	88	100
1000	2.8×10^{-3}	1.64	0.86	65	88	100
10,000	2.8×10^{-3}	1.64	0.86	65	88	100

535
 536
 537

538 5 Discussion

539 5.1 Runup Predictors

540 Studies of commonly used deterministic runup parameterizations such as those proposed by Hunt (1959),
541 Holman (1986) and Stockdon et al. (2006) amongst others, show that these parametrizations are not
542 universally applicable and there remains no perfect predictor of wave runup on beaches (Atkinson et al.,
543 2017; Passarella et al., 2018a; Power et al., 2018). This suggests that the available parametrizations do
544 not fully capture all the relevant processes controlling wave runup on beaches (Power et al., 2018). Recent
545 work has used ensemble and data-driven methods to account for unresolved factors and complexity in
546 runup processes. For example, Atkinson et al. (2017) developed a ‘model-of-models’ by fitting a least-
547 squares line to the predictions of several runup parameterizations. Power et al. (2018) used a data-driven,
548 deterministic, Gene-Expression Programming model to predict wave runup against a large dataset of
549 runup observations. Both of these approaches led to improved predictions, when compared to
550 conventional runup parameterizations, of wave runup on the datasets tested in these studies.

551

552 The work presented in this study used a data-driven Gaussian process (GP) approach to develop a
553 probabilistic runup predictor. While the mean predictions from the GP predictor developed in this study
554 using high-resolution LIDAR data of wave runup were accurate (RMSE = 0.18 m) and better than those
555 provided by the Stockdon et al. (2006) formula tested on the same data (RMSE = 0.36 m), the key
556 advantage of the GP approach over deterministic approaches is that probabilistic predictions are output
557 that are specifically derived from data and implicitly account for unresolved processes and uncertainty in
558 runup predictions. Previous work has similarly used GPs for efficiently and accurately quantifying
559 uncertainty in other environmental applications (e.g., Holman et al., 2014; Kupilik et al., 2018; Reggente
560 et al., 2014). While alternative approaches are available for generating probabilistic predictions, such as
561 Monte Carlo simulations (e.g., Callaghan et al., 2013), the GP approach offers a method of deriving
562 uncertainty explicitly from data, requires no deterministic equations, and is computationally efficient (i.e.,
563 as discussed in Sect. 4.3, drawing 10,000 samples of 120-hour runup time series on a standard desktop
564 computer took less than one second). However, as discussed in Sect. 2.3, when developing a GP, or any

565 machine learning model, the training data should include the full range of possible variability in the data
566 to be modelled in order to avoid extrapolation. A limitation of using this data-driven approach for runup
567 prediction is that it can be difficult to acquire a training dataset that captures all possible variability in the
568 system, from, for example, longer-term trends in the wave climate, extreme events or a potentially
569 changing wave climate in the future (Semedo et al., 2012).

570 **5.2 Including Uncertainty in Dune Erosion Models**

571 Uncertainty in wave runup predictions within dune-impact models can result in significantly varied
572 predictions of dune erosion. For example, the model of Larson et al. (2004) used in this study only predicts
573 dune erosion if runup elevation exceeds the dune toe elevation and predicts a non-linear relationship
574 between runup that exceeds the dune toe and resultant dune erosion. Hence, if wave runup predictions are
575 biased too low then no dune erosion will be predicted, and if wave runup is predicted too high then dune
576 erosion may be significantly over predicted. Ensemble modelling has become standard practice in many
577 areas of weather and climate modelling (Bauer et al., 2015), hydrological modelling (Cloke and
578 Pappenberger, 2009), and more recently has been applied to coastal problems such as the prediction of
579 cliff retreat (Limber et al., 2018) as a method of handling prediction uncertainty. While using a single
580 deterministic model is computationally simple and provides one solution for a given set of input
581 conditions, model ensembles provide a range of predictions that can better capture the variety of
582 mechanisms and stochasticity within a coastal system. The result is typically improved skill over
583 deterministic models (Atkinson et al., 2017; Limber et al., 2018) and a natural method of providing
584 uncertainty with predictions.

585

586 As a quantitative comparison, Splinter et al. (2018) applied a modified version of the LEH04 model to
587 the same June 2011 storm dataset used in the work presented here with a modified expression for the
588 collision frequency (i.e. the t/T term in **Eq. (9)**) based on work by Palmsten and Holman (2012). The
589 parameterization of Stockdon et al. (2006) was used to estimate R_2 in the model. The model was forced
590 hourly over the course of the storm, updating the dune toe, recession slope, and profiles based on each
591 daily LIDAR survey. Based on only the 40 profiles used in the present study, results from Splinter et al.

592 (2018) showed that the deterministic LEH04 approach reproduced 68% ($r^2 = 0.68$) of the observed
593 variability in dune erosion. As shown in **Table 1**, the simple LEH04 model (**Eq. (9)**) applied here using
594 the GP runup predictor to generate ensemble prediction reproduced ~85% (based on the ensemble mean)
595 of the observed variability in dune erosion for the 40 profiles. While there are some discrepancies in the
596 two modelling approaches, the ensemble approach clearly has an appreciable increase in skill over the
597 deterministic approach; attributed here to using a runup predictor trained on local runup data, and the
598 ensemble modelling approach. However, a major advantage of the ensemble approach over the
599 deterministic approach is the provision of prediction uncertainty (e.g., **Fig. 8**). While the mean ensemble
600 prediction is not 100% accurate, **Table 1** shows that using just 100 samples can capture all the observed
601 variability in dune erosion within the ensemble output.

602

603 The GP approach is a novel approach to building model ensembles to capture uncertainty. Previous work
604 modelling beach and dune erosion has successfully used Monte Carlo methods, which randomly vary
605 model inputs within many thousands of model iterations, to produce ensembles and probabilistic erosion
606 predictions (e.g., Callaghan et al., 2008; Li et al., 2013; Ranasinghe et al., 2012). As discussed earlier in
607 **Sect. 4.3**, the GP approach differs to Monte Carlo in that it explicitly quantifies uncertainty directly from
608 data, does not use deterministic equations, and can be computationally efficient.

609 6 Conclusion

610 For coastal managers, the accurate prediction of wave runup as well as dune erosion is critical for
611 characterizing the vulnerability of coastlines to wave-induced flooding, erosion of dune systems, and
612 wave impacts on adjacent coastal infrastructure. While many formulations for wave runup have been
613 proposed over the years, none have proven to accurately predict runup over a wide range of conditions
614 and sites of interest. In this contribution, a Gaussian process (GP) was used with over 8000 high-resolution
615 LIDAR-derived wave runup observations were used to develop a probabilistically parametrization of
616 wave runup that quantify uncertainty in runup predictions. The mean GP prediction performed well on
617 unseen data, with a RMSE of 0.18 m, a significant improvement over the commonly used R_2
618 parameterization of Stockdon et al. (2006) (RMSE of 0.36 m) used on the same data. Further, only 10
619 randomly drawn models from the probabilistic GP distribution were needed to form an ensemble that
620 captured 95% of the scatter in the test data.

621

622 Coastal dune-impact models offer a method of predicting dune erosion deterministically. As an example
623 application of how the GP runup predictor can be used in geomorphic systems, the uncertainty in the
624 runup parameterization was propagated through a deterministic dune erosion model to generate ensemble
625 model predictions and provide prediction uncertainty. The hybrid dune erosion model performed well on
626 the test data, with a squared-correlation (r^2) between the observed and predicted dune erosion volumes of
627 0.85. Importantly, the probabilistic output provided uncertainty bands of the expected erosion volumes
628 which is a key advantage over deterministic approaches. Compared to traditional methods of producing
629 probabilistic predictions such as Monte Carlo, the GP approach has the advantage of learning uncertainty
630 directly from observed data, it requires no deterministic equations, and is computationally efficient.

631

632 This work is an example of how a machine learning model such as a GP can profitably be integrated into
633 coastal morphodynamic models (Goldstein and Coco, 2015) to provide probabilistic predictions for
634 nonlinear, multidimensional processes and drive ensemble forecasts. Approaches combining machine
635 learning methods with traditional coastal science and management models present a promising area for
636 furthering coastal morphodynamic research. Future work is focused on using more data and additional

637 inputs, such as offshore bar morphology and wave spectra, to improve the GP runup predictor developed
638 here, testing it at different locations and integrating it into a real-time coastal erosion forecasting system.

639 **Code and Data Availability**

640 The data and code used to develop the Gaussian Process runup predictor in this manuscript are publicly
641 available at https://github.com/TomasBeuzen/BeuzenEtAl_GP_Paper.

642 **Author Contributions**

643 The order of the authors' names reflects the size of their contribution to the writing of this manuscript.

644 **Acknowledgements**

645 This research was partially funded by ongoing support by Northern Beaches Council, the Australian
646 Research Council (LP04555157, LP100200348, DP150101339) and the NSW Environmental Trust
647 Environmental Research Program (RD 2015/0128). Wave and tide data were kindly provided by Manly
648 Hydraulics Laboratory under the NSW Coastal Data Network Program managed by OEH. The lead
649 Author is funded under the Australian Postgraduate Research Training Program. EBG acknowledges
650 financial support from DOD DARPA (R0011836623/HR001118200064).

651 **References**

- 652 Atkinson, A. L., Power, H. E., Moura, T., Hammond, T., Callaghan, D. P., and Baldock, T. E.:
653 Assessment of runup predictions by empirical models on non-truncated beaches on the south-east
654 Australian coast, *Coastal Engineering*, 119, 15-31, 2017.
- 655 Bauer, P., Thorpe, A., and Brunet, G.: The quiet revolution of numerical weather prediction, *Nature*,
656 525, 47, 2015.
- 657 Berner, J., Achatz, U., Batté, L., Bengtsson, L., Cámara, A. d. I., Christensen, H. M., Colangeli, M.,
658 Coleman, D. R., Crommelin, D., and Dolaptchiev, S. I.: Stochastic parameterization: Toward a new
659 view of weather and climate models, *Bulletin of the American Meteorological Society*, 98, 565-588,
660 2017.
- 661 Beuzen, T., Splinter, K., Marshall, L., Turner, I., Harley, M., and Palmsten, M.: Bayesian Networks in
662 coastal engineering: Distinguishing descriptive and predictive applications, *Coastal Engineering*, 135,
663 16-30, 2018.
- 664 Birkemeier, W. A., Savage, R. J., and Leffler, M. W.: A collection of storm erosion field data, *Coastal*
665 *Engineering Research Center*, Vicksburg, MS, 1988.
- 666 Booij, N., Ris, R. C., and Holthuijsen, L. H.: A third-generation wave model for coastal regions: 1.
667 Model description and validation, *Journal of Geophysical Research: Oceans*, 104, 7649-7666, 1999.
- 668 Buchanan, M.: Ignorance as strength, 2018. Nature Publishing Group, 2018.
- 669 Callaghan, D. P., Nielsen, P., Short, A., and Ranasinghe, R.: Statistical simulation of wave climate and
670 extreme beach erosion, *Coastal Engineering*, 55, 375-390, 2008.
- 671 Callaghan, D. P., Ranasinghe, R., and Roelvink, D.: Probabilistic estimation of storm erosion using
672 analytical, semi-empirical, and process based storm erosion models, *Coastal Engineering*, 82, 64-75,
673 2013.
- 674 Camus, P., Mendez, F. J., Medina, R., and Cofiño, A. S.: Analysis of clustering and selection algorithms
675 for the study of multivariate wave climate, *Coastal Engineering*, 58, 453-462, 2011.
- 676 Cloke, H. and Pappenberger, F.: Ensemble flood forecasting: A review, *Journal of Hydrology*, 375, 613-
677 626, 2009.
- 678 Cohn, N. and Ruggiero, P.: The influence of seasonal to interannual nearshore profile variability on
679 extreme water levels: Modeling wave runup on dissipative beaches, *Coastal Engineering*, 115, 79-92,
680 2016.
- 681 Dancik, G. M. and Dorman, K. S.: mlegp: statistical analysis for computer models of biological systems
682 using R, *Bioinformatics*, 24, 1966-1967, 2008.
- 683 den Heijer, C., Knipping, D. T. J. A., Plant, N. G., van Thiel de Vries, J. S. M., Baart, F., and van
684 Gelder, P. H. A. J. M.: Impact Assessment of Extreme Storm Events Using a Bayesian Network,
685 Santander, Spain2012.
- 686 Erikson, L. H., Larson, M., and Hanson, H.: Laboratory investigation of beach scarp and dune recession
687 due to notching and subsequent failure, *Marine Geology*, 245, 1-19, 2007.
- 688 García-Medina, G., Özkan-Haller, H. T., Holman, R. A., and Ruggiero, P.: Large runup controls on a
689 gently sloping dissipative beach, *Journal of Geophysical Research: Oceans*, 122, 5998-6010, 2017.
- 690 Goldstein, E., Coco, G., and Plant, N. G.: A Review of Machine Learning Applications to Coastal
691 Sediment Transport and Morphodynamics. *EarthArXiv*, 2018.

692 Goldstein, E. B. and Coco, G.: A machine learning approach for the prediction of settling velocity,
693 Water Resources Research, 50, 3595-3601, 2014.

694 Goldstein, E. B. and Coco, G.: Machine learning components in deterministic models: hybrid synergy in
695 the age of data, Frontiers in Environmental Science, 3, 33, 2015.

696 Goldstein, E. B., Coco, G., and Murray, A. B.: Prediction of wave ripple characteristics using genetic
697 programming, Continental Shelf Research, 71, 1-15, 2013.

698 Goldstein, E. B. and Moore, L. J.: Stability and bistability in a one-dimensional model of coastal
699 foredune height, Journal of Geophysical Research: Earth Surface, 121, 964-977, 2016.

700 Guedes, R., Bryan, K. R., and Coco, G.: Observations of wave energy fluxes and swash motions on a
701 low-sloping, dissipative beach, Journal of geophysical research: Oceans, 118, 3651-3669, 2013.

702 Guza, R. and Feddersen, F.: Effect of wave frequency and directional spread on shoreline runup,
703 Geophysical Research Letters, 39, 2012.

704 Holman, D., Sridharan, M., Gowda, P., Porter, D., Marek, T., Howell, T., and Moorhead, J.: Gaussian
705 process models for reference ET estimation from alternative meteorological data sources, Journal of
706 Hydrology, 517, 28-35, 2014.

707 Holman, R.: Extreme value statistics for wave run-up on a natural beach, Coastal Engineering, 9, 527-
708 544, 1986.

709 Hunt, I. A.: Design of sea-walls and breakwaters, Transactions of the American Society of Civil
710 Engineers, 126, 542-570, 1959.

711 Krasnopolsky, V. M. and Fox-Rabinovitz, M. S.: Complex hybrid models combining deterministic and
712 machine learning components for numerical climate modeling and weather prediction, Neural
713 Networks, 19, 122-134, 2006.

714 Kupilik, M., Witmer, F. D., MacLeod, E.-A., Wang, C., and Ravens, T.: Gaussian Process Regression
715 for Arctic Coastal Erosion Forecasting, IEEE Transactions on Geoscience and Remote Sensing, 2018.
716 1-9, 2018.

717 Larson, M., Erikson, L., and Hanson, H.: An analytical model to predict dune erosion due to wave
718 impact, Coastal Engineering, 51, 675-696, 2004.

719 Li, F., Van Gelder, P., Callaghan, D., Jongejan, R., Heijer, C. d., and Ranasinghe, R.: Probabilistic
720 modeling of wave climate and predicting dune erosion, Journal of Coastal Research, 65, 760-765, 2013.

721 Limber, P. W., Barnard, P. L., Vitousek, S., and Erikson, L. H.: A model ensemble for projecting
722 multidecadal coastal cliff retreat during the 21st century, Journal of Geophysical Research: Earth
723 Surface, 123, 1566-1589, 2018.

724 MacDonald, B., Ranjan, P., and Chipman, H.: GPfit: An R package for fitting a Gaussian process model
725 to deterministic simulator outputs, Journal of Statistical Software, 64, 2015.

726 Mastrandrea, M. D., Field, C. B., Stocker, T. F., Edenhofer, O., Ebi, K. L., Frame, D. J., Held, H.,
727 Kriegler, E., Mach, K. J., and Matschoss, P. R.: Guidance note for lead authors of the IPCC fifth
728 assessment report on consistent treatment of uncertainties, 2010. 2010.

729 Mull, J. and Ruggiero, P.: Estimating storm-induced dune erosion and overtopping along US West
730 Coast beaches, Journal of Coastal Research, 30, 1173-1187, 2014.

731 Overbeck, J. R., Long, J. W., and Stockdon, H. F.: Testing model parameters for wave-induced dune
732 erosion using observations from Hurricane Sandy, Geophysical Research Letters, 44, 937-945, 2017.

733 Palmsten, M. L. and Holman, R. A.: Laboratory investigation of dune erosion using stereo video,
734 Coastal engineering, 60, 123-135, 2012.

735 Palmsten, M. L., Splinter, K. D., Plant, N. G., and Stockdon, H. F.: Probabilistic estimation of dune
736 retreat on the Gold Coast, Australia, Shore and Beach, 82, 35-43, 2014.

737 Parker, K., Ruggiero, P., Serafin, K. A., and Hill, D. F.: Emulation as an approach for rapid estuarine
738 modeling, Coastal Engineering, 2019. 2019.

739 Passarella, M., De Muro, S., Ruju, A., and Coco, G.: An assessment of swash excursion predictors using
740 field observations, Journal of Coastal Research, 85, 1036-1040, 2018a.

741 Passarella, M., Goldstein, E. B., Muro, S. D., and Coco, G.: The use of genetic programming to develop
742 a predictor of swash excursion on sandy beaches, Natural Hazards and Earth System Sciences, 18, 599-
743 611, 2018b.

744 Pedregosa, F., Varoquaux, G., Gramfort, A., Michel, V., Thirion, B., Grisel, O., Blondel, M.,
745 Prettenhofer, P., Weiss, R., and Dubourg, V.: Scikit-learn: Machine learning in Python, Journal of
746 machine learning research, 12, 2825-2830, 2011.

747 Phillips, M., Blenkinsopp, C., Splinter, K., Harley, M., and Turner, I.: Modes of berm and beachface
748 recovery following storm reset: observations using a continuously scanning lidar, Journal of
749 Geophysical Research: Earth Surface, 2019. 2019.

750 Plant, N. G. and Stockdon, H. F.: Probabilistic prediction of barrier-island response to hurricanes,
751 Journal of Geophysical Research: Earth Surface, 117, n/a-n/a, 2012.

752 Power, H. E., Gharabaghi, B., Bonakdari, H., Robertson, B., Atkinson, A. L., and Baldock, T. E.:
753 Prediction of wave runup on beaches using Gene-Expression Programming and empirical relationships,
754 Coastal Engineering, 2018. 2018.

755 Ranasinghe, R., Callaghan, D., and Stive, M. J.: Estimating coastal recession due to sea level rise:
756 beyond the Bruun rule, Climatic Change, 110, 561-574, 2012.

757 Rasmussen, C. E. and Nickisch, H.: Gaussian processes for machine learning (GPML) toolbox, Journal
758 of machine learning research, 11, 3011-3015, 2010.

759 Rasmussen, C. E. and Williams, C. K.: Gaussian Processes for Machine Learning, The MIT Press,
760 Cambridge, Massachusetts, 2006.

761 Reggente, M., Peters, J., Theunis, J., Van Poppel, M., Rademaker, M., Kumar, P., and De Baets, B.:
762 Prediction of ultrafine particle number concentrations in urban environments by means of Gaussian
763 process regression based on measurements of oxides of nitrogen, Environmental modelling & software,
764 61, 135-150, 2014.

765 Roberts, S., Osborne, M., Ebdon, M., Reece, S., Gibson, N., and Aigrain, S.: Gaussian processes for
766 time-series modelling, Phil. Trans. R. Soc. A, 371, 20110550, 2013.

767 Roelvink, D., Reniers, A., van Dongeren, A., van Thiel de Vries, J., McCall, R., and Lescinski, J.:
768 Modelling storm impacts on beaches, dunes and barrier islands, Coastal Engineering, 56, 1133-1152,
769 2009.

770 Ruggiero, P., Komar, P. D., McDougal, W. G., Marra, J. J., and Beach, R. A.: Wave runup, extreme
771 water levels and the erosion of properties backing beaches, Journal of Coastal Research, 2001. 407-419,
772 2001.

773 Sallenger, A. H.: Storm impact scale for barrier islands, Journal of Coastal Research, 2000. 890-895,
774 2000.

775 Semedo, A., Weisse, R., Behrens, A., Sterl, A., Bengtsson, L., and Günther, H.: Projection of global
776 wave climate change toward the end of the twenty-first century, *Journal of Climate*, 26, 8269-8288,
777 2012.

778 Short, A. D. and Trenaman, N.: Wave climate of the Sydney region, an energetic and highly variable
779 ocean wave regime, *Marine and Freshwater Research*, 43, 765-791, 1992.

780 Splinter, K. D., Kearney, E. T., and Turner, I. L.: Drivers of alongshore variable dune erosion during a
781 storm event: Observations and modelling, *Coastal Engineering*, 131, 31-41, 2018.

782 Splinter, K. D. and Palmsten, M. L.: Modeling dune response to an East Coast Low, *Marine Geology*,
783 329, 46-57, 2012.

784 Stockdon, H. F., Holman, R. A., Howd, P. A., and Sallenger, A. H.: Empirical parameterization of
785 setup, swash, and runup, *Coastal Engineering*, 53, 573-588, 2006.

786 Stockdon, H. F., Sallenger Jr, A. H., Holman, R. A., and Howd, P. A.: A simple model for the spatially-
787 variable coastal response to hurricanes, *Marine Geology*, 238, 1-20, 2007.

788 Tinoco, R., Goldstein, E., and Coco, G.: A data-driven approach to develop physically sound predictors:
789 Application to depth-averaged velocities on flows through submerged arrays of rigid cylinders, *Water*
790 *Resources Research*, 51, 1247-1263, 2015.

791 Van Oorschot, J. and d'Angremond, K.: The effect of wave energy spectra on wave run-up. In: *Coastal*
792 *Engineering 1968*, 1969.

793